Available online at www.sciencedirect.com
SCIENCE DIRECT
Journal of Catalysis 235 (2005) 35–51
JOURNAL OF CATALYSIS
www.elsevier.com/locate/jcat

Microkinetic modeling of propane aromatization over HZSM-5

Aditya Bhan, Shuo-Huan Hsu, Gary Blau, James M. Caruthers, Venkat Venkatasubramanian, W. Nicholas Delgass *

School of Chemical Engineering, Purdue University West Lafayette, IN 47907-1283, USA

Received 4 October 2004; revised 22 May 2005; accepted 11 July 2005

Available online 18 August 2005

Abstract

Reaction kinetic studies of propane conversion to aromatics were conducted on an HZSM-5 zeolite at a pressure of 1 atm, temperatures in the range 793–823 K, and different space times (0–12 g_{cat} h/mol). The rates of production of methane, ethane, ethene, propene, propane, butane, butene, benzene, toluene, and xylene are reported. A kinetic model has been postulated that considers surface species as neutral alkoxides, reactions of these alkoxide species by carbenium ion-like transition states, and alkane activation by carbonium ion-like transition states. The associated elementary steps, categorized within the reaction types adsorption, desorption, unimolecular protolytic cracking and dehydrogenation, β-scission, oligomerization, hydride transfer, alkylation, dealkylation, and cyclization, were parsed into reaction families based on an equal reactivity assumption. A total of 311 reaction steps were grouped into 37 reaction families, and the number of unknown parameters was reduced to 25 using adsorption parameters for n-alkanes and relative rates for β-scission and hydride transfer from the literature. It is proposed that this kinetic model describes the reaction behavior over an HZSM-5 catalyst in terms of relevant rate and equilibrium constants and activation energies.

Keywords: Kinetic modeling; Propane aromatization; HZSM-5; Elementary steps

1. Introduction

The activation and selective conversion of light (C_1–C_4) alkanes to aromatics and dihydrogen represent major challenges of catalytic chemistry. The complexity of aromatization chemistry makes it difficult to unravel reaction mechanisms; hence conclusions are drawn largely from experimental product distributions and kinetics interpreted in the context of carbocation chemistry. From a fundamental standpoint, elucidating the kinetics of this complicated system in terms of an elementary step mechanism parameterized in terms of rate and equilibrium constants would improve the understanding of the interactions of hydrocarbons with solid acids. In this article we report kinetic studies of propane conversion over an HZSM-5 catalyst at temperatures ranging from 793 to 823 K at varying space times ($W/F = 0$–12 g_{cat} h/mol) under nondeactivating conditions. We postulate an elementary step-based reaction mechanism for propane aromatization based on the following reaction types: adsorption and desorption, protolytic disproportionation and dehydrogenation of paraffins, hydride transfer, β-scission-oligomerization, alkylation, dealkylation, cyclization, and aromatization reactions. We group the elementary steps into various reaction families that are assumed to have equal reactivity. We further reduce the number of parameters (bounded by transition state theory for pre-exponential factors and literature values for relative energies), use experimental data to estimate the values for these parameters using a hybrid GA-based optimization procedure [1,2], and present sensitivity analyses with respect to the rate constants to show the degree to which the various parameters influence catalyst performance. This work is set in the context of the literature in the next section, which describes the model details.

* Corresponding author. Fax: +1-765-494-0805.
E-mail address: delgass@ecn.purdue.edu (W.N. Delgass).

0021-9517/$ – see front matter
doi:10.1016/j.jcat.2005.07.005

1.1. Background

1.1.1. Paraffin activation

Significant methane, ethane, and hydrogen production on cracking *n*-hexane or 3-methylpentane over HZSM-5 that could not be explained by the classical carbenium ion mechanism led Haag and Dessau [3] to postulate a monomolecular cracking mechanism involving carbonium ions, in analogy to superacid chemistry. The hypothesis was supported by the product distribution observed, with protonation occurring at the most highly substituted carbon atom for 3-methylpentane (3-MP). The penta-coordinated carbonium ion species was assumed to collapse into three pairs of products, each pair consisting of an alkane or dihydrogen and an adsorbed carbenium ion. When extrapolated to zero conversion, the product distribution observed for 3-MP included nearly equimolar amounts of dihydrogen, methane, and ethane, explaining the observed product distribution for 3-MP cracking.

Following the work of Haag and Dessau, a number of researchers confirmed the essential correctness of the protolytic cracking mechanism [4–13]. It is favored only at low alkene concentrations and low conversion. Because alkenes are better proton acceptors, higher olefin concentrations result in secondary reactions and predominance of carbenium ion chemistry at higher conversion rates. But recent quantum chemical studies have proposed the existence of different transition states for H/D exchange, dehydrogenation, and cracking [14–20] and have suggested that the idea of a single carbonium ion transition state is perhaps oversimplified.

1.1.2. Alkoxide intermediates

^{13}C magic angle spinning nuclear magnetic resonance (MAS NMR) experimental studies [21,22], as well as theoretical computational catalysis studies [23–28], have shown that the transformation of hydrocarbons in zeolites proceeds through the interaction of carbenium-ion-like species with basic lattice oxygen atoms resulting in covalently bonded surface alkoxy groups with only partially polarized carbonyl bonds rather than ion pairs. The short C–O bond length, tetrahedral H–O–C and C–C–C angles, and relatively low charge on the alkyl fragment computed by density functional theory (DFT) calculations also support the formation of alkoxide species [24,27–32]. Theoretical calculations also suggest that the transition states involve a polarization of the C–O bond and that the top of the potential barrier corresponds to carbenium ion-like species with significant ionic character.

1.1.3. Modeling approaches

Various approaches have been taken in developing kinetic models of hydrocarbon conversion processes over solid acid catalysts. One approach is to use pseudocomponent models in which species are compartmentalized based on similar physical and chemical properties, with the reaction network then defined in terms of chemical interaction between these compartments. Coarsely compartmental models often cannot be used to interpret the effects of catalyst properties on the phenomenological aspects of catalytic chemistry, because fundamental catalytic reaction mechanisms are not incorporated into the kinetic scheme. In addition, the actual composition of these compartments in terms of molecular components may alter the system kinetics. Quann and Jaffe [33] developed a method to describe the chemistry of complex hydrocarbon mixtures wherein individual hydrocarbon molecules are represented as a vector of incremental structural features. This vector representation, called structure-oriented lumping, provides a framework for constructing arbitrarily large and complex reaction networks and including molecular-based property correlations. This formalism enables composition-based modeling of very complex refinery processes; however, such complexity typically is not encountered for the light paraffin aromatization system, and hence most modeling studies have incorporated the catalyst structure into the kinetics in view of the simpler product distribution. Froment [34] described the generation of reaction networks using a computer algorithm in which each elementary step is calculated as the product of single events and the so-called “single event rate” coefficient. This approach has the advantage that the single event rate coefficient is independent of feedstock. Froment et al. successfully analyzed the catalytic cracking of *n*-paraffins using this approach [35,36].

Microkinetic analysis, a paradigm in heterogeneous catalysis popularized by Dumesic et al. [37], aims “to consolidate in a quantitative fashion available experimental data, theoretical principles, and appropriate correlations relevant to the catalytic process.” The fundamental starting point in microkinetic analysis is the formulation of elementary reaction steps that capture the essential surface chemistry involved in the catalytic reaction in terms of physical and chemical parameters that can be measured independently or that can be estimated by theoretical means. Dumesic, Madon, et al. [38–41] consolidated these concepts and presented sophisticated microkinetic studies for USY and β zeolites used as FCC catalysts under varying conditions.

In work directly related to the work presented here, Lukyanov and Shtral [42] described a simplified kinetic model for light olefin aromatization reaction over HZSM-5 zeolites with different aluminum content and pretreatment conditions. Lukyanov et al. [43] then extended the proposed kinetic scheme to describe ethene and propene aromatization over HZSM-5, and also included additional kinetic steps for Ga/HZSM-5-based catalysts. Equal reactivity assumptions that considered several related reactions to have the same rate constant and lump all isomeric species were used to reduce the number of parameters. The gallium sites were distinguished from the protonic sites of the zeolite. Based on a comparison of the model and the data, these authors concluded that the gallium ion-exchanged species did not participate in the initial steps of ethene and propene transformation and also did not affect the acidic sites of the parent zeo-

lite. Lukyanov et al. [44] extended the foregoing proposed formulation to describe propane aromatization over HZSM-5 and Ga/HZSM-5. The extension was achieved by adding new reaction steps corresponding to alkane adsorption and paraffin activation on acid and gallium catalytic sites. Paraffin activation was identified as the rate-determining step.

The model proposed by Lukyanov et al. [43–46] represents a valuable starting point in the kinetic modeling of paraffin aromatization; however, it provides only relative rate parameters. Because our philosophy for optimal catalyst formulation [47] relies extensively on the validity of the kinetic model, we have developed a detailed microkinetic model for paraffin aromatization. Rate constant and activation energy values are estimated for each of these reaction families, and experimental data are used to determine the significance of these parameters. In contrast to most of the approaches outlined earlier, we place significant emphasis on determining the appropriate grouping rules, as well as assigning the relative rates to various reaction families. Although our grouping scheme is not unique, it does develop a clear strategy for grouping reactions that should be widely applicable to a number of other hydrocarbon reaction systems.

1.1.4. Kinetic model development

The mechanism and kinetics of paraffin aromatization closely resonate with the mechanism of paraffin cracking on solid acid catalysts. An excellent review of kinetics of catalytic cracking was presented by Wojciechowski [48]. The model developed herein incorporates significant details from the catalytic cracking literature as well as features of microkinetic modeling as suggested by Dumesic et al.

The elementary step-based mechanism developed here involves adsorption, desorption, unimolecular protolytic cracking and dehydrogenation, β-scission, oligomerization, hydride transfer, alkylation, dealkylation, cyclization, and aromatization reactions. The reaction mechanism lumps all isomers together, to reduce the number of reacting species; hence it does not consider hydride and methyl shifts, and it restricts the carbon number of the reaction species to nine, because products larger than C_9 in any significant concentrations are not observed experimentally. The proposed scheme comprises 33 gas phase species and 35 surface species interacting in 311 reaction steps. These elementary steps are translated to a set of differential and algebraic equations using the reaction modeling suite [1,47]. Appendix A describes the procedure for generating the elementary steps used in this reaction scheme. To reduce the number of parameters, the equal reactivity assumption is used; reactions are categorized into various families, and all reactions in a particular family are assumed to have the same rate constant. The model contains 37 such reaction families, each of which is parameterized in terms of either a forward rate constant or a thermodynamic equilibrium constant that relates the forward and reverse rate constants for an elementary step. Using relative numbers from the literature and theoretical chemistry considerations, we further reduced the number of unknown parameters that must be estimated from experimental data; a detailed description of the parameterization scheme is given in Section 1.2.

Our model assumes that neutral surface alkoxy species react through carbenium ion-like transition states, whereas initiation reactions occur through carbonium ion-like transition states; thereby explaining why selectivity patterns are controlled by the relative stabilities of tertiary, secondary, and primary carbenium ions.

1.2. Parameterization scheme

The parameterization of the various reaction types presented herein represents just one of the many ways in which this reaction network could be parsed. Alternative parameterization schemes are a subject of ongoing research, but comparison of these schemes is not very intuitive, because they involve different numbers of parameters.

Each of the reaction families is initially parameterized in terms of a typical unimolecular or bimolecular pre-exponential factor and an activation barrier. In a well-documented approach to obtaining better estimates for the kinetic parameters involved [49], after a fit was obtained for the activation barrier and the pre-exponential factor as shown in Eq. (1), each parameter described below was reparameterized in terms of a rate constant at a reference temperature of 803 K and an activation barrier, as shown in (2). The initial estimates obtained for parameters in (1) were used to obtain narrow bounds on the k_{ref} values in (2). The rate constants for temperatures other than the reference temperature were determined as shown in (2):

$$k = A\exp\left(-\frac{E_{\mathrm{act}}}{RT}\right), \tag{1}$$

$$k_T = k_{\mathrm{ref}}\exp\left(-\frac{E_{\mathrm{act}}}{R}\left(\frac{1}{T}-\frac{1}{T_{\mathrm{ref}}}\right)\right). \tag{2}$$

1.2.1. Adsorption–desorption of alkanes

Calorimetric, gravimetric, and infrared studies have shown that alkanes preferentially physisorb onto Brønsted acid sites in HZSM-5 [27,50–53]. Significant nonbonding interactions also exist between the adsorbed alkane molecules and the zeolite [54–58]. These interactions depend primarily on the pore diameter and fit of the alkane molecule in the pore volume and have been found to be relatively independent of the composition of the molecular sieve [59–61]. The *Nest effect*, the ability of the physisorbed molecule to optimize its configuration with respect to the molecular sieve, was first postulated by Derouane et al. [54,55,62]. Coverage-dependent effects at high loadings, as well as differences between *n*- and iso-alkanes in the context of the nest effect, have been observed but were not considered in our model development, because we do not distinguish between structural isomers at the present stage. This is one of the many limitations of our model made for simplicity.

The heat of adsorption for *n*-alkanes has been observed to increase linearly with carbon number [51,53]; this increase has been attributed to the enhanced physical interactions of the additional alkyl groups with the zeolite lattice. Accordingly, we consider the heat of adsorption of alkanes to be comprised of physical van der Waals interactions, which increase linearly with carbon number, and specific interactions of the paraffin molecule with the Brønsted acid site, which are independent of carbon number.

In addition, a *compensation effect*—a linear increase in the heat of adsorption with increasing adsorption entropy—has been observed for *n*-alkane adsorption [53]. The adsorption–desorption characteristics of paraffin adsorption are represented by an equilibrium constant. Literature values for the adsorption enthalpy and the corresponding relationship that determines the compensation effect were used [53]. Hence, given a carbon number, the adsorption enthalpy, and hence the equilibrium constant, are explicitly determined, the uncertainties in these estimates are ignored, and no fitting parameters are involved. The calculated values for the equilibrium constants suggest that the adsorption phenomena are relatively independent of carbon number, because the increase in the heat of adsorption is accompanied by a corresponding increase in adsorption entropy.

1.2.2. Protolytic cracking

Protolysis is a unimolecular reaction in which an adsorbed paraffinic species is activated via a carbonium ion-like transition state and collapses into an adsorbed alkoxide species and an alkane. Ab initio quantum chemical calculations confirm this mechanism and suggest that the negatively charged lattice oxygen species greatly stabilize the positively charged transition state relative to the adsorbed intermediates, and hence a significant effect of cluster size (i.e., the number of lattice T atoms used for these computational studies) has been evaluated for these calculations [20]. Narbeshuber et al. [5] investigated the protolytic cracking of C_3–C_6 hydrocarbons on HZSM-5 and found that selectivity for protolysis of C_5H_{12} is temperature-independent. The apparent activation energy was found to decrease linearly with carbon number; however, after consideration of the enhanced heat of adsorption with increasing carbon number, the true activation energy was determined to be independent of carbon number. Babitz et al. [57] investigated the monomolecular cracking of *n*-hexane on Y, MOR, and ZSM-5 zeolites, and, within experimental error, attributed the differences in apparent activation energies to differences in heats of *n*-hexane adsorption, such that the intrinsic activation energies are identical. Thus the intrinsic rate for protolytic cracking appears to be independent of carbon number and zeolite type, and the observed differences in apparent rates arise primarily due to different adsorption behavior.

In our model, the 28 C–C bond cleavage reactions not resulting in the formation of a methoxide species were grouped under one reaction family parameterized in terms of two parameters: a pre-exponential factor with typical values for a unimolecular reaction and an activation energy with upper and lower bounds taken from the literature. Product distribution data suggest that protolytic cleavage resulting in formation of a methoxy species is slow compared with other protolytic steps (see Section 3). Hence a second reaction family comprising seven reactions that result in the collapse of a carbonium ion-like transition state to an alkane and a methoxy species was postulated. One additional parameter accounting for the higher relative activation energy for protolysis reactions involving the methoxy species was considered.

1.2.3. Protolytic dehydrogenation

Protolytic dehydrogenation refers to a unimolecular reaction that, like protolysis, proceeds through a carbonium ion-like transition state and results in an adsorbed alkoxide intermediate and an H_2 molecule. But experimental studies show that unlike in protolysis, in dehydrogenation the true activation energy is a function of carbon number [5]. The true activation energy for dehydrogenation increases with carbon number, and the increase in observed rate for dehydrogenation with increasing carbon number can be attributed to the elevated sorption constants with increasing carbon number. The dehydrogenation steps have been parameterized in terms of three parameters: a typical unimolecular pre-exponential factor, an activation energy bounded by literature values for a particular carbon number (C_3H_8 for this study), and the linear increase in true activation energy with increasing carbon number.

Experimental evaluation of protolytic mechanisms at short times on stream suggests that the rate of cracking exceeds the rate of dehydrogenation for C_3–C_6 with an increase in the relative rate of cracking with increasing carbon number [5]. Accordingly, a constraint requiring that the ratio of the rate constant of protolytic cracking to the rate constant for protolytic dehydrogenation (for C_3 and C_4) be within 1.5–4 at 803 K was imposed as a constraint during parameter estimation, to ensure that the parameter estimates were consistent with known results in the literature.

1.2.4. Alkene adsorption–desorption

For olefinic molecules, interaction with Brønsted acid sites often results in oligomerization, and hence experimental measurements for adsorption energies represent a challenge. In situ NMR and infrared spectroscopic studies, along with quantum chemical studies, have demonstrated that carbenium ions exist only as transition states, and that protonation of alcohols and alkenes results in alkoxide intermediates. Only some alkyl-substituted carbenium ions in which the positive charge is delocalized and sterically inaccessible to framework oxygens have been detected [63–67]. Alkene adsorption involves a physisorbed state wherein the olefin double bond interacts with the Brønsted acid proton, followed by a chemisorption step that involves, in a concerted manner, proton transfer from the Brønsted site to a carbon

atom of the olefin double bond and simultaneous C–O bond formation at the adjacent lattice oxygen [26,27,68,69].

Alkene physisorption does not involve an activation barrier, and the specific interaction energy is significantly stronger than that for the corresponding paraffinic molecules. Whether or not the nest effect is preserved in olefins as a consequence of this strong interaction remains an open question. The transition from the physisorbed state to the chemisorbed state is an activated process and occurs through a carbenium ion-like transition state.

Chemisorbed alkoxide intermediates figure in each of the 311 elementary steps in the proposed mechanism, whereas physisorbed olefin molecules are not explicitly accounted for because they are first transformed to alkoxide species before reaction. Formation of the chemisorbed alkoxide species has been described as a bimolecular step occurring between the gas phase olefin molecule and the Brønsted acid site. The adsorption mechanism is taken to be independent of carbon number and is parameterized in terms of two parameters: a bimolecular pre-exponential factor and an activation energy. The activation energy for the desorption reaction is constrained to be the activation energy of adsorption plus the heat of adsorption. The value of the energy of olefin adsorption is also considered an unknown parameter, bounded by values available from theoretical calculations [25–27,69,70].

1.2.5. β-scission–oligomerization

The activation energy for β-scission reactions changes significantly depending on the relative stability of the carbenium ion-like transition state. In treating the isomerization and hydrocracking of C_9–C_{16} paraffins over Pt/ZSM-5, Weitkamp et al. [71] introduced terminology that is useful in organizing the various types of carbenium ion β-scission reactions. Buchanan et al. [72] further extended this nomenclature and studied the relative rates of the various types of β-scission for C_5–C_8 olefins over ZSM-5 at 783 K under low hydrocarbon partial pressure and high silica/alumina ratios to minimize the effects of bimolecular reactions. For the model developed here, in cases where the reaction could be categorized in more than one reaction family had isomers been accounted for, the structure and reaction family whose contribution was expected to give the maximum rate were chosen. For example, a $3^\circ \rightarrow 2^\circ$ cleavage of an adsorbed C_7H_{14} species was considered to give C_4H_8 and an adsorbed C_3H_6 species; this reaction also could have been considered under $2^\circ \rightarrow 1^\circ$ β-scission. Buchanan et al. [72] experimentally observed that the product distribution was independent of the hexene or heptene isomer that was fed, indicating that double-bond and skeletal isomerization were facile and preceded significant cracking.

These seven reaction families were characterized by two parameters: a unimolecular pre-exponential factor and an activation energy for the β-scission of a 2° adsorbed alkoxide to a 1° adsorbed alkoxide and an alkene (see Appendix B). The relative rates between the various other reaction families were estimated from experimental data generated by Buchanan et al. [72]. Because these rates were determined at 783 K, the relative rates were translated to relative activation energies assuming identical pre-exponential factors, and these relative activation energy values were subsequently used to determine the temperature dependence of the rate constants (see Appendix B for details).

Oligomerization represents the reverse reaction of β-scission. A family of oligomerization reactions corresponds to each of the seven reaction families for β-scission. The forward and reverse rate constants are related by an equilibrium constant, and because the rate constants for β-scission were already estimated, the oligomerization reaction families were parameterized in terms of equilibrium relations. The ΔH values were calculated based on the standard tabulated values of heats of formation of 1-alkenes (when more than one isomeric structure could be postulated) and taking into consideration the heat of adsorption of the alkene. The ΔS value was considered a parameter for these families of reactions, because the model predictions were found to be very sensitive to this value. This parameter was bounded by the free gas phase entropy.

1.2.6. Hydride transfer

Kazansky et al. computationally investigated the mechanism of hydride transfer on 1T and 3T zeolite cluster models incorporating one and three tetrahedral Si or Al atoms, respectively [73,74]. Accordingly, the mechanism for hydride ion transfer starts with the alkane attacking the C–O alkoxy bond of the adsorbed intermediate, resulting in a considerable increase in the C–O bond distance and in the charge separation of the adsorbed alkoxide species and the surface. Enhanced substitution at the central carbon atom increases the stability of the carbenium ion-like fragments formed on charge separation and decreases the energy of activation. The short-lived intermediate, as postulated by Kazansky et al., closely resembles the nonclassical penta-coordinated carbonium ion. The 59 hydride transfer steps in the proposed mechanism have been categorized into 12 reaction families based on the relative stabilities of the postulated transition state complexes and the reactants and products (see Appendix B for details).

Kazansky et al. also computed five examples of hydride transfer [73,74]. These consist of two examples of primary to primary (methoxy and methane, ethoxy and ethane) and one example each of secondary to secondary (propoxy and propane), tertiary to tertiary (iso-butoxy and iso-butane), and tertiary to secondary (iso-butoxy and propane). Because these small clusters introduce termination effects and also neglect the influence of long-range electrostatic effects caused by the Madelung potential, the absolute numbers based on these computations cannot be considered; however, we assume that the relative numbers have relevance. In addition, because the relative numbers for all 12 reaction families are not available, based on the carbon number of the two reactant species and the nature (primary, sec-

ondary, or tertiary) of the chemisorbed intermediate, the 12 reaction families were grouped in terms of the 4 reaction families for which the relative rate numbers were available from the work of Kazansky et al. Three of the reaction families include hydride transfer with olefins as reactants. To our knowledge, these hydrogen transfer steps have yet not been studied in the quantum chemical literature; however, these successive hydrogen transfer steps are required for conversion of an olefin such as 1-hexene to an aromatic molecule such as benzene. These 12 reaction families were parameterized in terms of two independent parameters: a typical bimolecular pre-exponential factor and an activation energy for a particular reaction family, with relative activation energies considered from the work of Kazansky et al. We note that parsing the 12 reaction families down to 4 is done on the basis of the nature of the alkoxide species formed, as well as in consideration of the volume of the intermediate involved; for example, tertiary to tertiary was considered inhibited due to steric factors. However, this particular parsing scheme may need to be refined in future improvements of the model.

1.2.7. Alkylation–dealkylation

Corma et al. [75,76] used quantum chemistry to investigate the mechanism of hydrocarbon transformation involving the formation and rearrangement of carbocationic intermediates. Theoretical studies of bimolecular reactions between carbenium ions and paraffins in the absence of the zeolite cluster by Boronat et al. [75,76] suggest the existence of a common intermediate for hydride transfer, disproportionation, dehydrogenation, and alkylation. This intermediate species closely resembles a nonclassical carbonium ion species, and different intramolecular rearrangements of this common intermediate have been postulated to explain the mechanism of the aforementioned acid-catalyzed hydrocarbon reactions. These calculations were extended to study hydrocarbon reactions in presence of the zeolite cluster by investigating the different processes that the $(C_2H_5–H–C_2H_5)^+$ carbonium ion interacting with a 3T cluster could undergo using the ab initio correlated MP2 and the density functional B3PW91 methods [76]. The $(C_2H_5–H–C_2H_5)^+$ cation, formed from adsorbed ethene and ethane, is evaluated to decompose into an *n*-butane molecule and to regenerate the Brønsted acid site, the global process being a paraffin–olefin alkylation reaction. Accordingly, an alkylation step was added to the reaction network, and the 33 reactions were grouped into two reaction families. Similar to the protolysis reactions described earlier, alkylation reactions involving a surface methoxy species were assumed to have higher activation barriers. These two reaction families were parameterized in terms of three parameters: a typical bimolecular pre-exponential factor, an activation energy, and a relative activation energy for reactions involving the methoxy species. For the alkylation reaction type, we chose to include only those reactions for which the sum of carbon numbers of the two reactant species was <10.

Alkylation of aromatic molecules by adsorbed C_1–C_3 alkoxy intermediates to result in larger aromatic molecules (smaller than C_{10}) and regenerate the Brønsted acid site was also considered within the aforementioned two reaction families. We note that alkylation reactions of aromatic molecules are perhaps more facile than that of alkanes, because alkylation of aromatics involves the interaction of the alkoxide species with a π-acceptor, whereas alkylation of alkanes involves the interaction of the alkoxide species with a sigma-donor alkane molecule. For the purposes of our current model, however, in an effort to reduce the number of parameters involved, we have chosen not to acknowledge this description.

The acid-catalyzed disproportionation of alkylbenzenes, particularly the selective toluene disproportionation to para-xylene exploiting the shape-selective characteristics of ZSM-5, has been extensively investigated in the literature. A review of the extensive literature is beyond the scope of this work, and the reader is referred to two review publications [77,78] for a broader discussion of this topic. Based on kinetic studies [79], H/D isotopic experiments [80], and DFT studies [81,82], three different mechanisms for toluene disproportionation have been proposed; it has been postulated that more than one mechanism may operate under different reaction conditions. For our model, we consider the C–C bond cleavage of alkylbenzenes resulting in surface alkoxides as the mechanism of dealkylation. The aforementioned alkylation reactions of aromatic molecules coupled with these dealkylation reactions represent the disproportionation reactions of alkylaromatics.

Experimentally observed product distributions show a higher production of toluene compared with xylene. Hence dealkylation of toluene was considered to have a higher activation barrier with respect to C_8 and C_9 alkylaromatics (see Section 3). The dealkylation of alkylbenzenes was grouped under a single reaction family parameterized in terms of three parameters: a unimolecular pre-exponential factor, an activation energy for C_8 and C_9 alkylaromatics, and a relative activation barrier accounting for the slower dealkylation of toluene.

1.2.8. Cyclization and aromatization

Dehydrocyclization, the conversion of light olefins to aromatics is often carried out over bifunctional catalysts containing acidic and dehydrogenation components. However, cyclization and aromatization reactions are also known to occur on purely acidic zeolites. It is postulated that the cyclization reaction involves an equilibrium between 5- and 6-membered ring species [83,84]. The existence of persistent cyclopentenyl and benzenium cations for MTG chemistry over HZSM-5 was clearly shown by Haw et al. [64,66,85,86]. However, 5-membered ring species were not observed in any significant concentration in the product distribution. In addition, the product distribution indicated that benzene, toluene, and xylenes (B/T/X) accounted for $>90\%$ of the aromatic products formed, and hence, for the model devel-

oped herein, we assumed that five aromatic species—B/T/X, ethylbenzene, and C_9H_{12}—were the only aromatic products formed, an additional limitation of our model. Cyclization was modeled as an elementary step wherein a protonated diene (carbon number $\geqslant 6$) was considered to go from an acyclic species to a cyclic adsorbed species (see Section 3). Based on recent theoretical calculations by Joshi et al. [87–89], C_6 cyclization was considered to have a 30 kJ/mol higher activation barrier than C_7 and C_8 cyclization. The cyclization reaction is parameterized in terms of a unimolecular pre-exponential factor and an activation energy for C_7 and higher carbon numbers. Desorption of the cyclized precursor is considered to give a cyclic monoene that is then assumed to undergo hydride transfer in a sequential manner in a reaction known as aromatization. The adsorbed aromatic species can subsequently desorb to give aromatic products, and no further cracking of the adsorbed aromatic species has been considered. The aromatization reaction has been parameterized in terms of two parameters: a typical bimolecular pre-exponential factor and an activation energy.

1.3. Parameter estimation

Ascertaining the validity of a complex model, as described earlier, is based on the quality of the experimental data generated during the course of this investigation and the credibility of the many literature sources referenced herein. The uncertainty in the parameter estimates generated from these literature sources was not included in subsequent data analysis and could result in biased results. Accommodating this uncertainty is left as an exercise for future modeling efforts. The physicochemical and mathematical complexity of the postulated model, which includes 25 unknown and highly correlated parameters, made estimation of these parameters from experimental data difficult. For parameter estimation, we used the reaction modeling suite (RMS), a suite of systems, optimization, and artificial intelligence tools developed for generating kinetic models and estimating parameters [1,90]. Given the chemistry rules and a set of experimental data, RMS generates the elementary reactions and the corresponding differential and algebraic equations, fits the parameters, and evaluates parameter sensitivity for the model. Unfortunately, RMS does not yet suggest additional experiments through which the quality of the parameter estimates could be improved.

Estimating parameters in a model consisting of a complex differential algebraic equation (DAE) system entails the problem of generating false parameter estimates when least squares or likelihood criteria are used to fit the model to experimental data. The only way to ensure convergence of these iterative nonlinear parameter estimation procedures to the correct set of parameter estimates is to supply the program with physicochemically meaningful parameter initial guesses that are reasonably close to the true estimates. Doing this proved a formidable challenge. It was not possible to generate such a set of good guesses because of the paucity of information in the literature and the experimental difficulties in trying to generate sets of data in which the various controlling parameters dominated and could be estimated in isolation from other competing species. This experimental limitation forced us to resort to an ad hoc procedure using genetic algorithms that do not guarantee a good starting guess but do explore large expanses of the 25-dimensional parameter space in a search for good starting guesses. Once these candidate 25-dimensional vectors of initial guesses were found, a classical Levenberg–Marquardt indirect search algorithm was used to generate the best nonlinear least squares parameter estimates in this region of parameter space. Such a procedure resulted in several sets of statistically equivalent sets of parameter estimates. These were tested by simulating behavior in the ranges: temperature 723–823 K, propane pressure 0–1 atm, and W/F 0–100 $g_{cat}\,h/mol$, and 15 solutions yielded surface concentrations $\geqslant 0$ and sums of squares within 10% of the optimal solution. Most of these solutions gave closely spaced parameter estimates that were reasonable physiochemically. We present the minima that resulted in the lowest sum of the squares fit. Additional modeling and experimental strategies to distinguish between these various minima are currently under investigation in our group.

The selection of a statistically meaningful fitting criterion is essential before parameter estimation can be initiated. This selection must reflect the type and location of uncertainty in the experimental data. For example, it is reasonable that concentration measurements with lower variability have greater information content than concentration measurements with higher variability, and hence the former should be "weighted" more heavily in estimating the model parameters. Much like a chemistry model is postulated to describe the reaction kinetics, a probabilistic model is needed to describe the uncertainty in the experimental data. The parameters of this probabilistic model of the data can be estimated from replicate experiments (i.e., two or more runs performed under exactly the same experimental conditions) and used to weight the data properly. Such data have been included in the experimental data set.

Assuming that the errors in the concentration measurements of component i, C_i, at space time τ are independently and normally distributed with mean 0 and known variance $\sigma_{i\tau}^2$, the best least squares parameter estimates, $\hat{k}$, are obtained by minimizing the least squares function

$$\sum_{i\tau} \left(\left(C_{i\tau} - \hat{C}_{i\tau}(\hat{k}) \right) / \sigma_{i\tau} \right)^2,$$

where $\hat{C}_{i\tau}(k)$ is the concentration of component i corresponding to space time τ predicted by the kinetic model using parameters $\hat{k}$. In this formulation each residual $e_{i\tau}(k) = C_{i\tau} - \hat{C}_{i\tau}(k)$ (i.e., the difference between the experimentally observed and mathematically calculated values) is weighted by the experimental standard deviation, which can be determined from the replicate measurements. To simplify the analysis and permit graphical interpretation of the data, we looked at two limiting cases:

(1) Sum of squared errors:

$$\mathrm{SS_E}(k) = \sum_i \bigl(C_i - \hat{C}_i(k)\bigr)^2,$$

where the weights or standard deviations are the same for all concentrations and for all space times.

(2) Sum of squared relative errors:

$$\mathrm{SS_{RE}}(k) = \sum_i \left(\frac{C_i - \hat{C}(k)_i}{C_i}\right)^2,$$

where the weights are proportional to the magnitude of the measurements or, stated alternatively, where the percent error in the measurements is constant. This of course corresponds to minimizing the sum of squares of the logarithms of the experimental and calculated values.

Because a constant percent error more closely resembles our experimental setup, we used $\mathrm{SS_{RE}}(k)$ for our modeling studies. This ensures that species with lower concentrations are treated the same as species with high concentration provided that the assumption of constant percent error is true. It will be an exercise for future work to relax this assumption and weight the data by the standard deviations obtained from replicate experiments. Another study will focus on estimating the parameters in various probability distributions and relating them to the kinetic model parameters.

1.3.1. Sensitivity analysis

A variety of techniques have been developed to investigate the sensitivity of complex kinetic systems [91,92]. In this work we use 95% confidence intervals and the degree of rate control as defined by Campbell [93].

Assuming no interaction or synergism between the parameters the confidence interval for each of p parameters $k_1, k_2, \ldots, k_p$ defined for a linear model is defined as [94]

$$\hat{k}_j - t_{\alpha/2,N-p}\mathrm{se}\bigl(\hat{k}_j\bigr) \leq k_j \leq \hat{k}_j + t_{\alpha/2,N-p}\mathrm{se}\bigl(\hat{k}_j\bigr), \tag{3}$$

where N is the number of data points, p is the number of parameters, and $t_{\alpha/2,N-p}$ is the upper $(100\alpha/2)\%$ point of the student-t distribution with $(N-p)$ degrees of freedom. The confidence limits for nonlinear models can be determined exactly only using Monte Carlo methods [95,96]. In this paper we have chosen to follow conventional but approximate nonlinear parameter estimation techniques and calculate asymptotic standard error for (3) by the following equation:

$$\mathrm{se}(k_j) = \hat{\sigma}\sqrt{\Gamma_{jj}}, \tag{4}$$

where

$$\hat{\sigma} = \sqrt{\frac{\sum_{i=1}^{N}(\ln C_i - \ln \hat{C}_i)^2}{N-p}} \tag{5}$$

and

$$\boldsymbol{\Gamma} = \bigl(\mathbf{J}^T\mathbf{J}\bigr)^{-1}, \quad J_{ij} = \left(\frac{\partial e_i}{\partial k_j}\right), \quad e_i = C_i - \hat{C}_i.$$

A small confidence interval indicates that either the model is inadequate to describe the particular feature characterized by the parameter or the parameter estimate is well defined or highly correlated with another parameter. The degree of rate control as defined by Campbell [93] can be used to determine the rate-limiting step in the reaction network.

1.3.2. Lack-of-fit test

The lack-of-fit test is a standard statistical technique [97] for determining the adequacy of the regression model. It assumes normality, independence, and constant variance of the residuals. The hypotheses for the test are as follows:

$\mathrm{H_0}$: There is no lack of fit between the model and the data.
$\mathrm{H_1}$: There is a lack of fit between the model and the data.

The traditional statistical treatment of testing the null hypothesis ($\mathrm{H_0}$) is the F-test, which involves partitioning the error or residual sum of squares ($\mathrm{SS_E}$) into two components, pure error ($\mathrm{SS_{PE}}$) and lack of fit ($\mathrm{SS_{LOF}}$):

$$\mathrm{SS_{PE}} = \sum_{i=1}^{m}\sum_{j=1}^{n_i}(y_{ij} - \bar{y}_i)^2, \tag{6}$$

$$\mathrm{SS_{LOF}} = \mathrm{SS_E} - \mathrm{SS_{PE}}, \tag{7}$$

where n_i is the number of replicates of the ith operating condition, $\mathbf{x}_i = (T, \mathbf{C}_0 \text{ and } W/F)_i$, m is the number of different levels of x_i, and $y_{ij} = \ln C_{ij}$, $\bar{y}_i = \frac{1}{n_i}\sum_{j=1}^{n}\ln C_{ij}$. The test procedure is as follows:

1. Calculate the test statistic F_0:

$$F_0 = \frac{\mathrm{MS_{LOF}}}{\mathrm{MS_{PE}}} = \frac{\mathrm{SS_{LOF}}/(m-p)}{\mathrm{SS_{PE}}/(n-m)}, \tag{8}$$

where p is the number of parameters.

2. If $F_0 > f_{\alpha,m-p,n-m}$ ($f_{\alpha,m-p,n-m}$ is the f-distribution), then we can conclude that the lack of fit is statistically significant and the model is not appropriate. α is the significance level before the test is performed, usually chosen as 0.01 or 0.05, and the confidence level is $100(1-\alpha)\%$.

3. P value is the value of α obtained by solving

$$F_0 = f_{\alpha,m-p,n-m}, \tag{9}$$

using the actual fit between the model and the experimental data. This P value can be used to calculate the confidence level $100(1-P)$ at which one can reject the null hypothesis and there is significant lack of fit.

In our case, the calculated P value is <0.001 (see Table 3), which means the probability that the model describes the data is $<1/1000$. We conclude that the lack of fit is statistically significant, and therefore the null hypothesis is rejected. Hence the model does not capture all the features of the system.

2. Experimental

HZSM-5 samples (Si/Al = 16 as measured by atomic absorption and ICP-AES) were obtained from ExxonMobil. X-ray diffraction (XRD) patterns obtained for the fresh catalyst confirmed the crystal structure of the material. Transmission electron microscopy (TEM) measurements averaged over several crystallites gave a crystallite diameter of 375 ± 125 nm. Surface area and pore volume measurements on a Micromiretics ASAP 2000C apparatus gave a BET surface area of 323.5 ± 5.9 m^2/g and a micropore volume of 0.134 cm^3/g. Although the BET formalism is not strictly valid for microporous materials, these measurements confirm the porosity of the material. ^{27}Al MAS NMR spectra referenced to the signal of a hydrated Al^{3+} cation in an octahedral environment $(Al(H_2O)_6)^{3+}$ showed the absence of extra-framework aluminum species. The zeolitic samples were first hydrated over saturated NH_4Cl solution in a dessicator at 80% relative humidity for 1 week, which was necessary to observe well-developed NMR signals [98]. Although the existence of aluminum species that reversibly convert from octahedral to tetrahedral symmetry on treatment with mild bases has been proposed [99], we note that Müller et al. [100], in their comparative study of dealumination of various zeolite types, did not observe any extraction of aluminum from the framework for HZSM-5 on calcination at 823 K. Because we do not observe any characteristics of extra-framework aluminum species in our ex situ characterization and do not subject the material to temperatures above 823 K, we consider the catalyst to contain only Brønsted acid sites. We also note that Ivanova et al. [101] did not observe any correlation between ^{13}C scrambling in labeled propane and the concentration of Lewis acid sites, suggesting that Brønsted acid sites may play a dominant role in this system.

Kinetic measurements were carried out in a continuous flow reactor at atmospheric pressure. The zeolite was sieved to 50–70 mesh and packed into a ½-inch o.d. quartz tube reactor placed in a vertically mounted Lindberg Blue furnace. A sheathed K-type thermocouple was placed in the reactor bed and sealed from the surrounding atmosphere by a Cajun™ adapter. The reactor was fed through Brooks 5850 mass flow controllers, and the reactor manifold was set up to send flow to either the reactor or the vent. Flows were calibrated with a bubble meter in the vent stream. The different space–time values were obtained by changing the amount of catalyst and feeding a constant flow rate of propane. Blank reactor studies confirmed the absence of homogeneous gas phase reactions. Five different catalyst weights (0.2, 0.4, 0.6, 0.8, and 1.0 g) were used, and data were generated for each amount at four different temperatures (793, 803, 813, and 823 K). Based on rate constant values for protolytic cracking and dehydrogenation obtained from parameter estimation ($k_{\text{Protolysis}} = 3.0$ (1/s) and $k_{\text{Dehydrogenation}} = 1.91$ (1/s); see Section 3), a one-dimensional plate geometry as proposed by Haag et al. [102], a typical diffusivity of 10^{-4} cm^2/s (even though, as discussed by Haag et al., the diffusivities in microporous materials often exceed those expected within the Knudsen regime), and a crystallite radius of 200 nm, the Thiele modulus was calculated to be <0.01. Hence, in agreement with Haag et al., we considered this reaction system to be kinetically controlled. The original conditions were restored at the end of each experimental run, and no significant deactivation effects or time-on-stream behaviors were observed. Repeat experiments for the entire data set at 803 and 813 K were conducted on fresh samples to confirm the reproducibility of the data, and these data were also used for parameter estimation and lack-of-fit testing. All products were analyzed with an Agilent 6890A series gas chromatograph, with a 30 m, 0.53-mm o.d. J&W Scientific GS-Alumina (115-3532) capillary column connected to a thermal conductivity detector (TCD) and a flame ionization detector (FID) in series.

3. Results and discussion

All 10 products (CH_4, C_2H_6, C_2H_4, C_3H_6, C_3H_8, C_4H_8, C_4H_{10}, B, T and X) quantified in the experimental measurements were used for parameter estimation. Data at all four temperatures and each of the five W/F values for each temperature were fitted simultaneously to estimate the 25 model parameters while the other parameter values were held constant at their literature estimated values. Figs. 1–4 show the model predictions for data at 793, 803, 813, and 823 K. Table 1 lists the parameters involved in terms of k_{ref} and activation barriers, the optimal fitted parameters, and the 95% confidence interval for the parameters involved. These are the parameters that passed the viability test discussed earlier. Because we use $\ln(k_{\text{ref}})$ as actual fitting parameters because of the scale of the parameters, the confidence intervals of k_{ref} values are not symmetric. It is seen that the energy parameters have tight confidence intervals, whereas the rate constant values at the reference temperature of 803 K have relatively large confidence intervals, particularly for bimolecular reactions. We ascribe this large variance to correlation between the reference rate constant value and the activation energy parameter, as well as to the uncertainty associated with considering a single value for the pre-exponential factor for entire bimolecular reaction families in the current parameterization scheme. Figs. 1–4 show that the model captures most of the behavior of the system; however, the P value calculated for our model (Table 3) suggests that the model does not capture all of the characteristic features of the data. Current efforts toward model refinement are aimed at incorporating low W/F and different partial pressure data.

According to the kinetic model, the surface of HZSM-5 is composed mostly of vacant acid sites under reaction conditions for propane conversion; that is, >98.5% of the acid sites are unoccupied under all reaction conditions. A similar observation was reported by Sanchez-Castillo et al. [40] for isobutane conversion over USY zeolite.

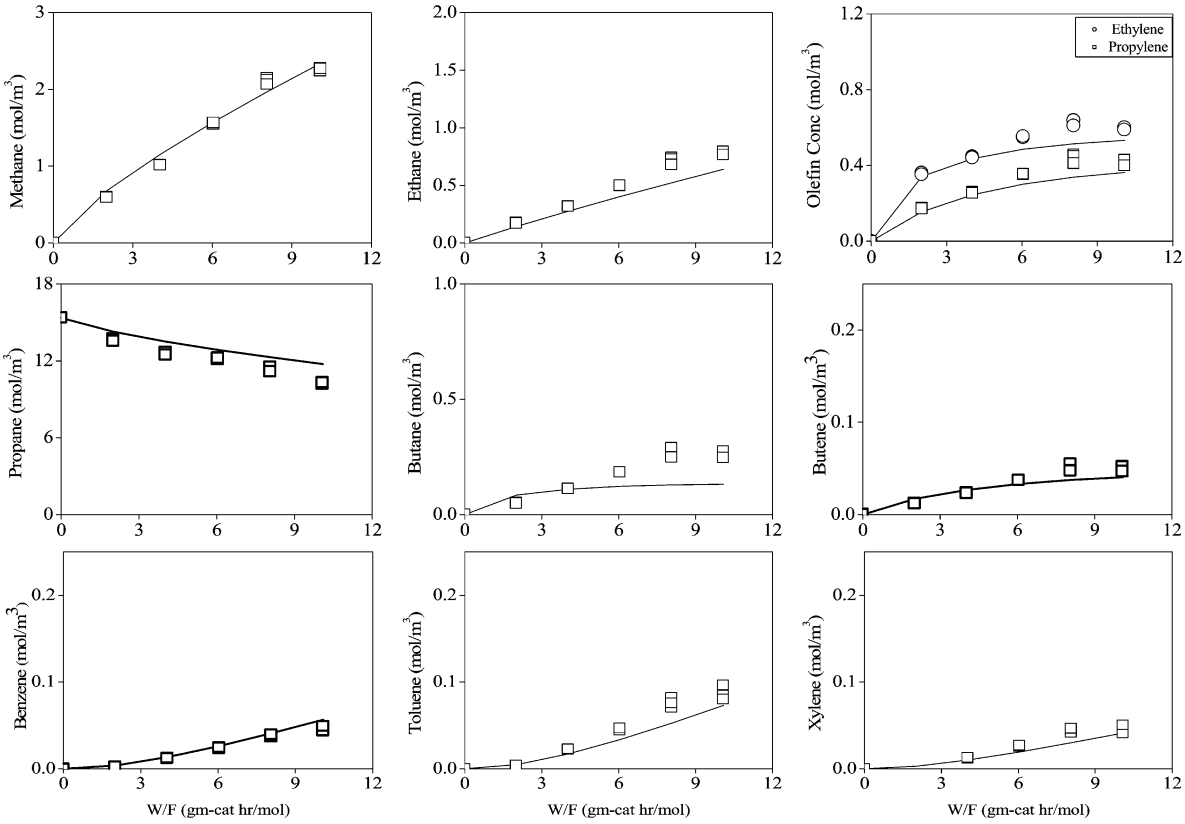

Fig. 1. Model predictions at $T = 793$ K. Predictions of the kinetic model are given by solid lines and experimental data are given by the open symbols.

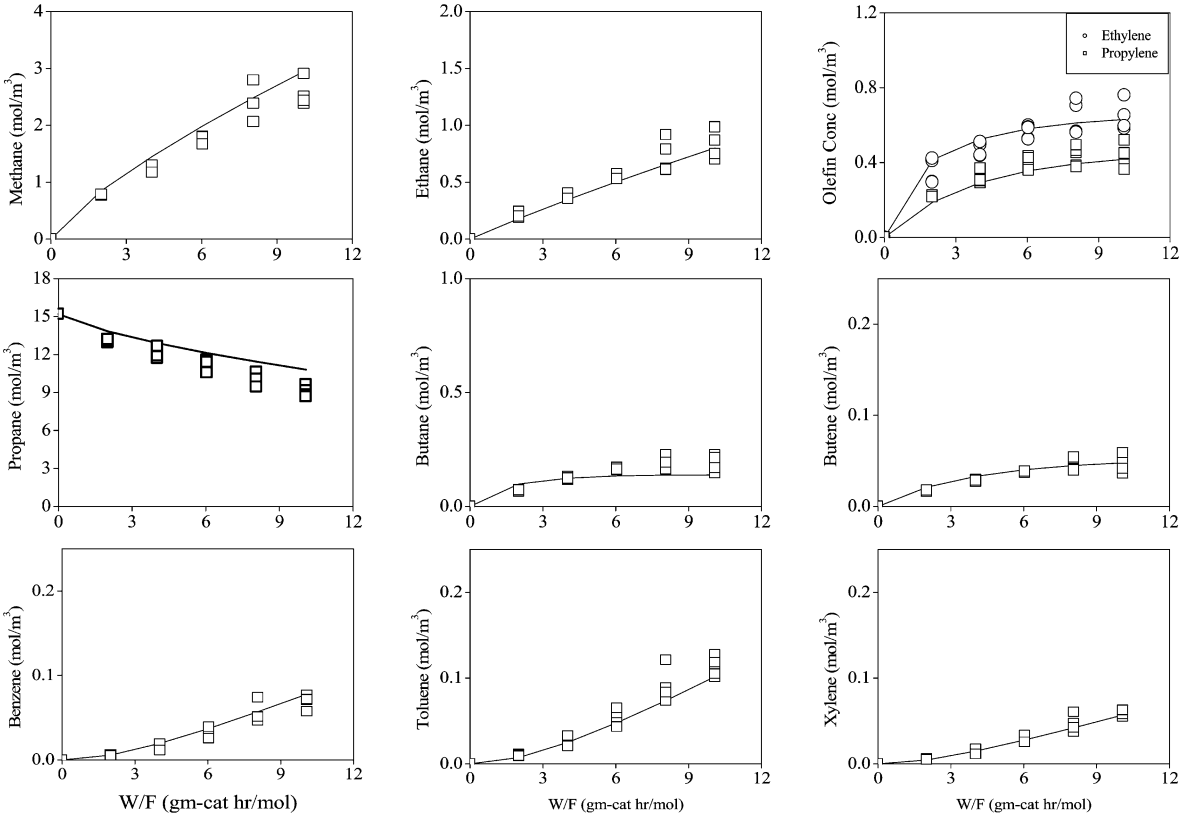

Fig. 2. Model predictions at $T = 803$ K. Predictions of the kinetic model are given by solid lines and experimental data are given by the open symbols.

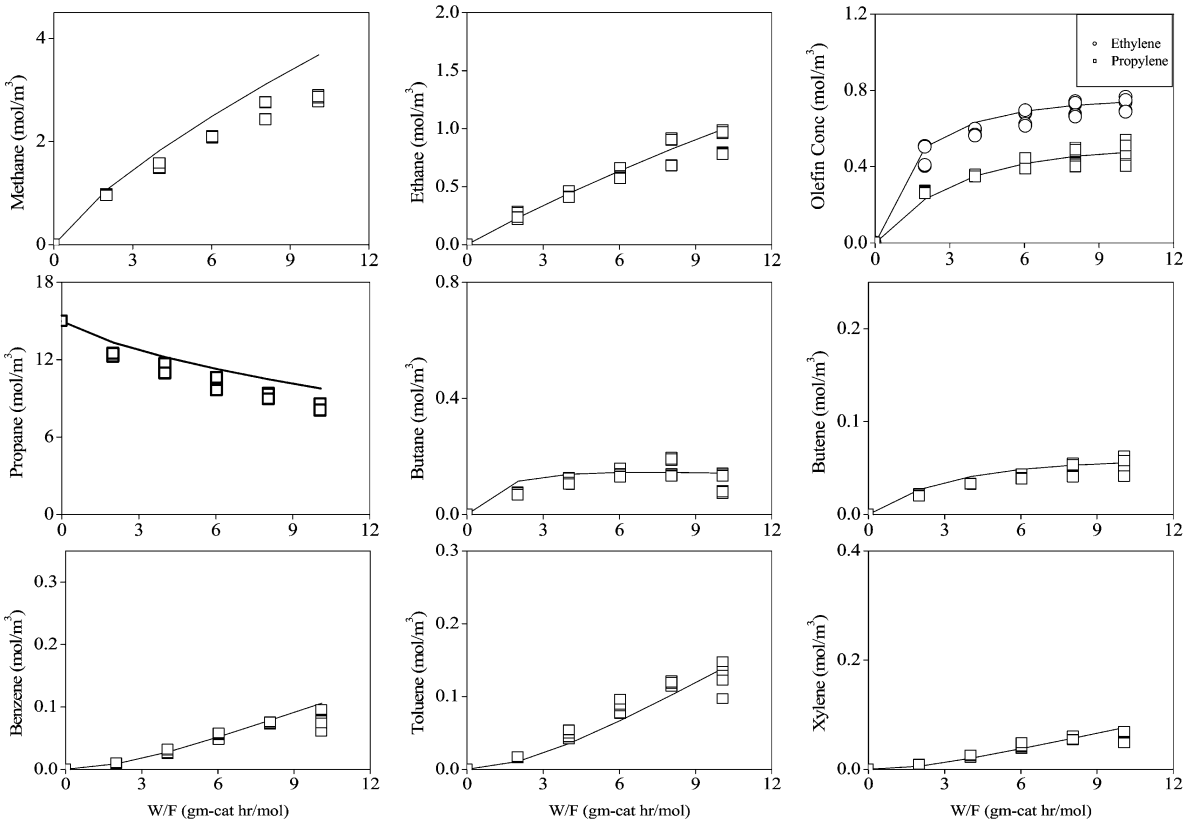

Fig. 3. Model predictions at $T = 813$ K. Predictions of the kinetic model are given by solid lines and experimental data are given by the open symbols.

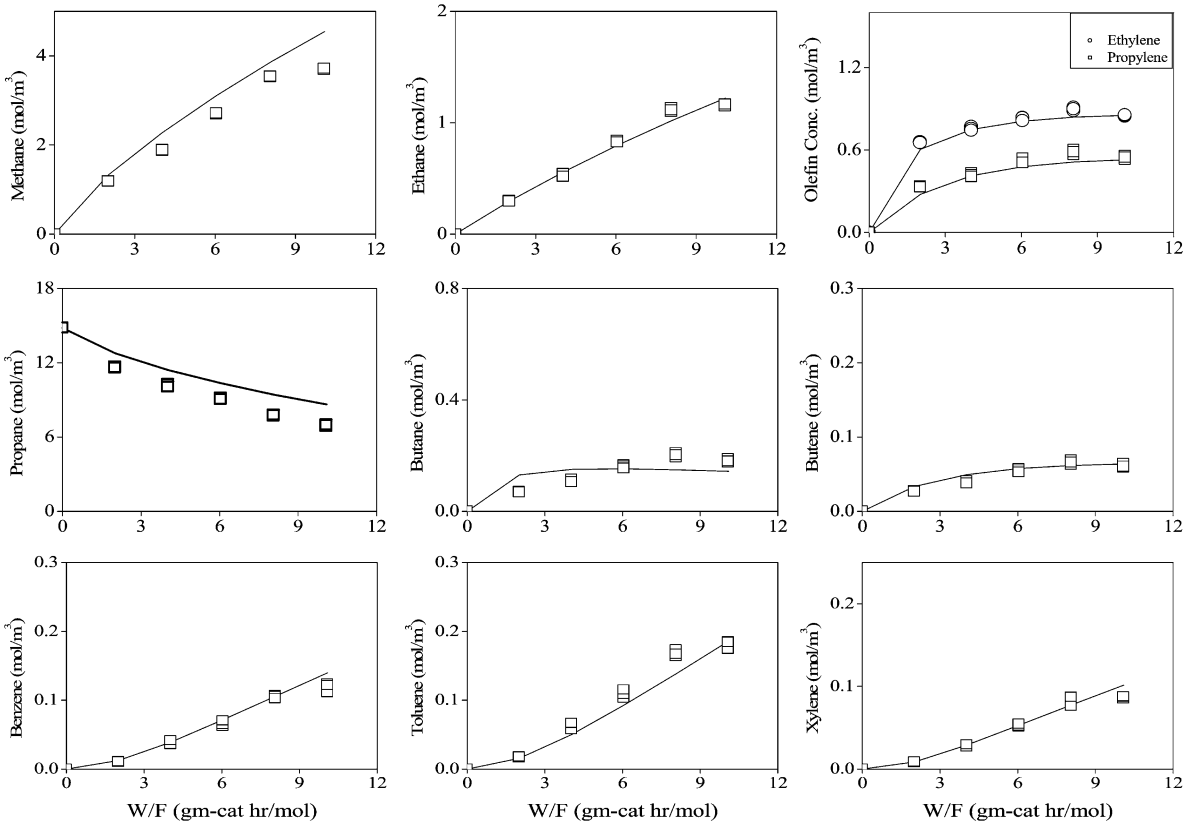

Fig. 4. Model predictions at $T = 823$ K. Predictions of the kinetic model are given by solid lines and experimental data are given by the open symbols.

Table 1
Optimal kinetic parameter values and 95% confidence limits at the reference temperature of 803 K[a]

Reaction type	Parameter	Optimal parameter value	95% confidence limit	
Protolysis	k_{ref}	3.0 (2.1×10^{14})	2.6	3.5
	E_{act}	212.7	212.6	212.8
	ΔE_{act}	12.0	9.7	14.4
Dehydrogenation	k_{ref}	1.91 (3.7×10^{10})	1.50	2.44
	E_{act}	158.2	158.0	158.3
	ΔE_{act}	0.8	0.7	0.9
Beta-scission	k_{ref}	516.4 (6.6×10^{10})	157.4	1694.5
	E_{act}	124.6	124.0	125.2
Dealkylation	k_{ref}	8.0×10^{-3}	4.0×10^{-4}	1.63×10^{-1}
	E_{act}	172.1 (1.25×10^{9})	171.0	173.3
	ΔE_{act}	30.1	27.9	32.3
Alkene chemisorption	k_{ref}	9.83×10^{-7} (1.3)	8.43×10^{-7}	1.15×10^{-6}
	E_{act}	94.0	93.8	94.2
Alkene desorption	k_{ref}	2.65 (3.6×10^{10})	1.78	3.94
	ΔH	61.8	61.5	62.2
Alkylation	k_{ref}	1.2×10^{-5} (1.6×10^{2})	5.3×10^{-6}	2.8×10^{-3}
	E_{act}	109.3	107.5	110.9
	ΔE_{act}	2.6	0.9	4.3
Aromatization	k_{ref}	4.63 (4.3×10^{2})	0.009	2419.2
	E_{act}	30.3	28.0	32.6
Hydride transfer	k_{ref}	3.87×10^{-5} (1.6×10^{1})	4.95×10^{-7}	3.03×10^{-3}
	E_{act}	86.2	85.3	87.2
Oligomerization	$\Delta S/R$	15.6	14.0	17.2
Cyclization	k_{ref}	9.7×10^{7} (1.2×10^{10})	9.7×10^{6}	9.7×10^{8}
	E_{act}	32.3	32.0	32.5

[a] Unimolecular rate constants (protolysis, dehydrogenation, beta-scission, dealkylation, alkene desorption, cyclization) are in (1/s), bimolecular rate constants (alkene chemisorption, alkylation, hydride transfer) are in (1/(Pa s)), activation energy and enthalpy values are in (kJ/mol) and the entropy parameter has been normalized by the universal gas constant (J/(mol K)). The following unit conversion for unimolecular steps was employed for the above rate parameters: Rate (mols/g_{cat} h) = k_{ref} (1/s) · θ (molecules/site) · (sites/g_{cat}) · (mols/molecule) · (s/h). A similar expression can be written for bimolecular steps. The value in the parentheses lists the pre-exponential factor in (1/s) or (1/(Pa s)) for each k_{ref} value at 803 K.

A significant emphasis of this work has been developing a systematic rationale for grouping reactions that is particularly relevant for understanding the kinetics of hydrocarbon systems comprising numerous reactions. Our rationale for parsing the reaction network is that similar reactants go to similar products through similar transition states and hence similar rate constants. This methodology is evident when examining the grouping of β-scission and hydride transfer reactions (see Appendix B).

We note that for protolytic cracking and alkylation reactions, we have postulated separate reaction families for reactions involving methoxy species, because reactions involving the methoxy (CH_3O^-) species constitute a special case. Carbenium ion mechanisms of acid catalyzed hydrocarbon reactions originally formulated and developed for homogeneous catalysis strongly discriminate against the formation of primary carbenium ions, because of their relative instability with respect to secondary and tertiary carbocations. For this reason, it has been generally postulated in the literature that a CH_3^+ species does not exist. In zeolite chemistry, however, alkoxide intermediates exist that do not follow the relative ordering observed in carbenium ion species in solutions [27,68,87,103]. In addition, ^{13}C MAS NMR has demonstrated the existence of methoxy (CH_3O^-) species bonded to the zeolite lattice [101,104,105]. Ethane has also been shown to be a primary product in several kinetic studies of propane aromatization. A protolysis step that considers the breakup of an adsorbed propane species to ethane and a methoxy species would account for these experimental observations. Isotopic tracer studies of propane reactions on HZSM-5 [106] have found that the ethane isotopic distribution closely resembles that of ethene. Those authors suggested that ethane is produced by the hydrogenation of ethylene; however, hydrogenation is not a reaction known to be facile on H-based zeolite catalysts, except under very high hydrogen partial pressures. We believe that this experimental observation could also be accounted for by considering the protolysis step described earlier combined with the fast H/D isotope scrambling. Model predictions were observed to improve once a higher activation barrier for

reactions involving methoxy species was included. Although it is evident that these reactions proceed through a primary carbocationic transition state, it also may be speculated that the methoxy species have a different local electronic configuration, because no C–C bonds are involved.

Table 1 shows that the activation barriers calculated for protolytic cracking and dehydrogenation agree very well with those reported by Narbeshuber et al. [5] for *n*-alkane activation over HZSM-5. The pre-exponential factor according to the transition state theory is specified as

$$A = \frac{kT}{h}\exp\left(\frac{\Delta S^{0\dagger}}{R}\right). \tag{10}$$

Based on k_{ref} values obtained for protolytic cracking and protolytic dehydrogenation, we calculated the pre-exponential factor and hence the change in entropy from the adsorbed precursor state to the transition state. We calculated the pre-exponential factor for cracking as 2.1×10^{14} (1/s), corresponding to a small entropy gain, and the pre-exponential factor for dehydrogenation as 3.7×10^{10} (1/s), with a corresponding entropy loss of 50.8 J/(mol K). Based on transition state structures for unimolecular cracking and dehydrogenation postulated by Lercher et al. [107], we ascribe the greater entropy loss for dehydrogenation to a much closer resemblance of the transition state structure to the alkoxide product state structure. Relative to the weakly held physisorbed alkane, the alkoxide is held much more strongly, and hence the entropy loss can be attributed to a loss in translational freedom (∼50 J/(mol K) per degree of translational freedom). On the other hand, the transition state structure for protolytic cracking does not resemble that for the stable alkoxide species and hence results in a small entropy gain. Our results also agree with those of Narbeshuber et al. [5], who also postulated a significantly greater entropy loss for dehydrogenation than for protolytic cracking.

The activation barrier regressed for β-scission (2° → 1°) when converted to a 2° → 2° β-scission reaction (see Appendix B for details) is calculated as 104.6 kJ/mol, which compares favorably with the value of 115.1 ± 5.7 kJ/mol reported by Sanchez-Castillo et al. [40,41] for isobutane conversion over USY, MOR, and zeolite β. But our rate-constant value for the β-scission reaction is lower than that reported by Dumesic et al., suggesting that entropy loss is greater for the β-scission reaction in the smaller pores of HZSM-5 compared with USY, MOR, and zeolite β.

The activation barrier calculated for 1° → 2° hydride transfer, when converted to 2° → 3° hydride transfer, is 69.6 kJ/mol. This also compares favorably with the 71.5 ± 0.6 kJ/mol computed by Dumesic et al. for hydride transfer of $C_{>5}$ species on zeolite β [40,41]. Hydride transfer reactions between 3° → 3° as well as those involving C_4 and larger olefins forming adsorbed allylic species have been inhibited by using a higher activation energy to account for the additional steric hindrance encountered by such species. We find the alkylation and hydride transfer processes to be kinetically competitive, with the rate constant for hydride transfer greater than that for alkylation in the reference hydride transfer reaction family considered. A similar conclusion was reported by Corma et al. [76] based on a DFT computational study. We note, however, that the activation barriers predicted differ considerably (∼20–25 kcal/mol from our study vs. ∼40 kcal/mol predicted by DFT studies), and ascribe these differences to the small size of the cluster (3T) used for the DFT studies. A carbocationic transition state such as the one postulated for alkylation and hydride transfer reactions is expected to be stabilized by lattice oxygen atoms, as was shown by Zygmunt et al. [20] for ethane cracking on HZSM-5.

Our results suggest that cyclization is a rapid process and is not the rate-limiting step for aromatization. Our calculated activation barrier for cyclization agrees well with embedded-cluster DFT results for C_6 and C_7 cyclization studies in HZSM-5 [88,89], and our mechanism for cyclization is in agreement with that proposed by Meriaudeau and Naccache on metal free zeolitic systems [84]. We note that although stable cyclopentenyl and benzenium carbenium ions have been shown to exist in MTG chemistry over HZSM-5, there is also evidence for cyclopentenyl cations with diverse substitution patterns [64,66,86]. In addition, theoretical studies for gas phase species [86,87] have also predicted a high energy barrier for cyclization through a tertiary carbenium ion species. Although the formation of hexatriene and thermal cyclization has been noted for noble metal catalysts, we seek to distinguish the mechanism for cyclization over acidic zeolites from bifunctional noble metal catalysts that have a high propensity to form metallocycloalkane intermediates and are efficient for aromatization. Although the possibility of cyclization through a protonated triene species exists, we note that because cyclization is very facile, a protonated diene is more likely to cyclize than to further dehydrogenate to form a triene. Although the recent work of Joshi and Thomson [88,89] did not investigate cyclization through a protonated triene, we surmise that additional conformational rigidity would be involved for ring closure inside the zeolite cavity with the presence of an additional double bond. The question that then arises is whether an acyclic diene is easier to dehydrogenate than a cyclic monoene. We conjecture that the cyclic monoene may be easier to dehydrogenate, because secondary carbocations are formed. Considering the foregoing observations, we note that the aromatization step in our mechanism is simply a hydride transfer of C_6–C_9 species with dienic or higher unsaturation with an alkoxide species. If cyclization within the zeolite were to occur through a triene species, then the aromatization step would still have to incorporate the dehydrogenation of the diene by successive hydride transfer steps to form a triene, as well as subsequent dehydrogenation steps of the cyclized diene. No significant alteration of the aromatization step would be required, whereas the cyclization step would need to shift from a dienic species to a protonated triene.

We note that the model predicts the B/T/X ratio in close agreement with experimental observations. The lower pro-

Table 2
$\sum_i |X_{RC,i}|$ calculated for different reaction types at $T = 793$ and 823 K at two different W/F values

Reaction type	$T = 793$ K		$T = 823$ K	
	$W/F = 5.42$ g_{cat} h/mol	$W/F = 27.12$ g_{cat} h/mol	$W/F = 5.63$ g_{cat} h/mol	$W/F = 28.14$ g_{cat} h/mol
Protolysis	0.66	0.63	0.63	0.61
Beta-scission	0.03	0.09	0.12	0.24
Hydride transfer	0.56	0.56	0.53	0.53
Olefin adsorption	0.23	0.06	0.18	0.02
Aromatization	–	–	–	–
Dehydrogenation	0.23	0.22	0.25	0.25
Alkylation	0.04	0.05	0.02	0.06
Dealkylation	–	–	–	–
Cyclization	–	–	–	–

duction of benzene is adequately explained by the 30 kJ/mol-higher activation energy for C_6 cyclization and is consistent with experimental observations of toluene and xylene as the initial aromatic products with subsequent production of benzene on dealkylation. Because C_7 cyclization and C_8 cyclization have similar activation barriers, the lower production of xylene could be accounted for by the faster dealkylation of C_8 and C_9 alkylaromatics compared with C_7 alkylaromatics. Based on the foregoing chemical reasoning and subsequent parameterization, we calculate a 30 kJ/mol-higher activation energy for C_7 dealkylation, which adequately accounts for the greater production of toluene.

Table 2 lists the absolute values of the degree of rate control for the various reaction types ($\sum_i |X_{RC,i}|$) at 793 and 823 K at two different values of space time. The most significant kinetic steps are those involving the initial activation of propane (protolysis and dehydrogenation) and hydride transfer steps, particularly the reaction family involving propane as the paraffinic reactant. No significant differences are observed in the narrow temperature range. Reactions such as dealkylation and cyclization are determined to not be kinetically significant under the conditions studied. Because the overall rate for calculating the degree of rate control is considered to be the rate of propane consumption, we believe that the low degree of rate control of the secondary reactions may stem from the fact that these reactions are not directly involved in propane consumption or formation. In a complex series—parallel reaction network like the one described here, how to probe the degree of rate control of these secondary reactions is not intuitively obvious to us.

Based on our modeling results, alkane activation is the slowest mechanistic step. Based on isotopic labeling studies of C_3H_8/C_3D_8 and C_3H_8/D_2 mixtures, however, the recombinative desorption of H-adatoms has also been suggested as the rate-limiting step [106,108]. The appearance of D-atoms in the reaction products is considered to represent C–D and H–D bond activation, with D_2 dissociation constituting the microscopic reverse of recombinative hydrogen desorption. The calculated virtual pressure of hydrogen was 216 kPa, whereas the gas phase pressure was <1 kPa [109]. However, these studies do not provide evidence for the nature of the adsorbed hydrogen species on the surface of the acidic catalyst. In addition, if hydrogen recombinative desorption were rate-limiting, then the observed reaction order for propane would be zero, but most experimental studies observe first-order kinetics. We note that H–D scrambling, taken to be representative of H–H and C–H bond activation, does not represent the rate of the dehydrogenation reaction, as discussed below.

Table 3
Analysis of variance for the lack-of-fit test

	Degree of freedom	Sum of squares	Mean square	F_0	P-value
Residual	922	38.94			
Pure error	748	3.58	0.0048	42.39	<0.001
Lack of fit	174	35.36	0.2031		

Recent experimental and theoretical work has sought to reconcile hydrogen–deuterium isotope exchange, protolytic dehydrogenation, and protolytic cracking occurring through penta-coordinated carbonium ion-like transition states and with widely different activation barriers and reaction rates by proposing different carbonium ion-like transition states for these reactions [107]. The H/D isotope exchange experiments of Narbeshuber et al. [110,111] confirmed that the rate of H/D exchange is about an order of magnitude faster than the rate of protolytic dehydrogenation or cracking. Theoretical studies by Blaszkowski and van Santen [14,18,112] and Esteves et al. [113] illustrated the very different nature of the transition state for H/D exchange and dehydrogenation. Although we agree with the aforementioned isotopic studies that adding a metallic component increases the reversibility of the dehydrogenation reaction, we propose that the experimental observations for the isotopic labeling studies on HZSM-5 are a result of facile H/D exchange of the reactant and product species with the zeolite.

Model predictions illustrated in Figs. 1–4 show that as temperature increases, the production of CH_4 increases, indicating that the protolytic cracking has a high activation barrier consistent with our model predictions. In addition, production of light alkenes like C_2H_4 and C_3H_6 lines out, consistent with the rapid conversion of these alkenes to higher-carbon-number products by oligomerization reac-

tions, as our model predicts. Our model also predicts that aromatics are secondary products (reflected in the initial slope of the curve), again consistent with experimental observations. We note that the greatest discrepancy between the model predictions and the experimental data are observed for butane, which the model does not capture adequately, and propane, which the model underpredicts. In an effort to understand why the model underpredicts the conversion of propane, we calculated the contribution of each species to the sum of squared logarithmic errors, our chosen objective function. This partial sum of squares error (PSSE) methodology reveals that the contribution of propane to a total SSE of 38.94 (see Table 3) was only 1.45. The highest contributions were from butane (PSSE = 12.25), toluene (6.52), and butene (4.06). Hence, based on our chosen objective function, we conclude that the disagreement between the experimental values and the model-predicted values for propane does not contribute significantly to the SSE, and the model does not attempt to fit the propane data better. As discussed earlier, an objective function weighted by the error of each experimental data point based on replicate measurements could address this scenario. Our attempts to improve the butane fit to significantly reduce the SSE have not been successful. We note, however, that butane production was overestimated by the model at short space-time conditions. An attempt to reduce the initial production of butane was another reason to slow the alkylation reaction involving methoxy species as reactants, because alkylation of propane by a methoxy species generates butane. Our current efforts are focused on changing the relative rates of alkylation and hydride transfer reactions resulting in the overprediction of butane at small (W/F) values.

In summary, although statistical evidence suggests scope for model refinement and treatment of error, the good agreement between experimental results and model predictions over a wide range of space time, and hence conversions, along with the good agreement between the kinetic parameters obtained and those published in the literature for similar hydrocarbon systems, suggest that we have developed a microkinetic model for this system that can describe the activity of Brønsted acid sites in HZSM-5.

4. Conclusions

An elementary step-based kinetic model that assumes neutral surface alkoxide species reacting through carbenium ion-like transition states and considers alkane activation by carbonium ion-like transition states has been postulated for propane aromatization on HZSM-5. This model acknowledges the carbon number dependence of alkane adsorption energetics, considers the existence and reaction of methoxy species, proposes a methodology for grouping reactions based on the nature (1°, 2°, or 3°) and size of the reaction intermediate for β-scission and hydride transfer reactions, and postulates elementary steps for cyclization and subsequent aromatization by hydride abstraction reactions. Model parameter estimates for protolytic alkane activation, β-scission, hydride transfer, and cyclization agree with literature values, and narrow confidence intervals are obtained for all energetic parameters in the model. Based on sensitivity analysis, we conclude that ring-closure and subsequent hydride transfer reactions to yield aromatic species are facile, whereas alkane activation steps are rate-controlling.

Acknowledgments

The authors thank Yogesh V. Joshi, Gowri Krishnamurthy, Kendall T. Thomson and Thomas F. Degnan Jr. for valuable discussions. Financial support for this work was provided by the Department of Energy, Office of Basic Energy Sciences, through Catalysis Science grant DE-FG02-03ER15466. The authors are grateful to ExxonMobil Refining and Supply for supplying the HZSM-5 catalyst used in this study.

Appendix A. Generation of the reaction scheme

The kinetic model for light paraffin aromatization on HZSM-5 has been derived on the basis of the following reaction steps. In the scheme below HS represents a Brønsted acid site, surface species are represented as $c_n h_m s$ and gas phase species are represented as $C_n H_m$.

1. Adsorption/desorption of paraffins (1 reaction family):
   $C_n H_{2n+2} + HS \leftrightarrow c_n h_{2n+3} s \quad (3 \leqslant n \leqslant 9)$.
2. Protolytic cleavage of paraffin molecules (2 reaction families):
   $c_n h_{2n+3} s \rightarrow C_m H_{2m+2} + c_{(n-m)} h_{2(n-m)+1} s$
   $(3 \leqslant n \leqslant 9$ and $1 \leqslant m < n)$.
3. Protolytic dehydrogenation of alkanes (1 reaction family):
   $c_n h_{2n+3} s \rightarrow c_n h_{2n+1} s + H_2 \quad (3 \leqslant n \leqslant 9)$.
4. Olefin adsorption including dienes and aromatics (1 reaction family):
   $C_n H_{2n} + HS \rightarrow c_n h_{2n+1} s \quad (2 \leqslant n \leqslant 9$; stoichiometry shown only for alkenes).
5. Olefin desorption including dienes and aromatics (1 reaction family):
   $c_n h_{2n+1} s \rightarrow C_n H_{2n} + HS \quad (2 \leqslant n \leqslant 9$; stoichiometry shown only for alkenes).
6. β-scission (7 reaction families):
   $c_n h_{2n+1} s \rightarrow c_m h_{2m+1} s + C_{(n-m)} H_{2(n-m)}$
   $(3 \leqslant n \leqslant 9$ and $1 \leqslant m < n)$.
7. Oligomerization (7 reaction families):
   $c_m h_{2m+1} s + C_{(n-m)} H_{2(n-m)} \rightarrow c_n h_{2n+1} s$
   $(3 \leqslant n \leqslant 9$ and $1 \leqslant m < n)$.

8. Hydride transfer (12 reaction families):

$c_m h_{2m+1}s + C_n H_{2n+2} \rightarrow C_m H_{2m+2} + c_n h_{2n+1}s$
$(1 \leqslant n, m \leqslant 9 \text{ and } m + n \leqslant 12)$,

$c_m h_{2m+1}s + C_n H_{2n} \rightarrow C_m H_{2m+2} + c_n h_{2n-1}s$
$(1 \leqslant m \leqslant 9; 4 \leqslant n \leqslant 9 \text{ and } (m + n) \leqslant 12)$.

9. Alkylation (2 reaction families):

$C_n H_{2n+2} + c_m h_{2m+1}s \rightarrow C_{(n+m)} H_{2(n+m+1)} + HS$
$(2 \leqslant n \leqslant 7; 1 \leqslant m \leqslant 7 \text{ and } (n + m) \leqslant 9)$,

$A + c_n h_{2n+1}s \rightarrow A\text{–}C_n H_{2n} + HS$
$(A = B/T/X; 1 \leqslant n \leqslant 3)$.

10. Dealkylation of alkylbenzenes (1 reaction family):

$B\text{–}c_n h_{2n+1}s \rightarrow B\text{–}C_m H_{2m} + c_{(n-m)} h_{2(n-m)+1}s$
$(0 \leqslant m \leqslant n; 1 \leqslant n \leqslant 3)$.

11. Cyclization and aromatization an accelerated hydride transfer process (2 reaction families):

$c_n h_{2n-1}s \rightarrow c_n h_{2n-1}s\_c \quad (6 \leqslant n \leqslant 9; \text{cyclization})$,

$c_n h_{2n-1}s\_c \rightarrow C_n H_{2n-2} + HS \quad (\text{Olefin desorption})$,

$c_m h_{2m+1}s + C_n H_{2n-2} \rightarrow C_m H_{2m+2} + c_n h_{2n-3}s$
$(6 \leqslant n \leqslant 9; 1 \leqslant m \leqslant 4 \text{ and } (n + m) \leqslant 12)$
(Aromatization reation).

Appendix B. Interrelationships used to reduce number of parameters

Interrelationships between various reaction families for β-scission/oligomerization and hydride transfer are specified below.

B.1. β-scission/oligomerization

$k\ (2^\circ \rightarrow 1^\circ) = \text{reference: estimated by optimization;}$
$k\ (1^\circ \rightarrow 1^\circ) = k\ (2^\circ \rightarrow 1^\circ) \times \exp(-4.6 \times 10^3/(RT));$
$k\ (1^\circ \rightarrow 2^\circ) = k\ (2^\circ \rightarrow 1^\circ);$
$k\ (2^\circ \rightarrow 2^\circ) = k\ (2^\circ \rightarrow 1^\circ) \times \exp(20.0 \times 10^3/(RT));$
$k\ (2^\circ \rightarrow 3^\circ) = k\ (2^\circ \rightarrow 1^\circ) \times \exp(27.4 \times 10^3/(RT));$
$k\ (3^\circ \rightarrow 2^\circ) = k\ (2^\circ \rightarrow 1^\circ) \times \exp(27.4 \times 10^3/(RT));$
$k\ (3^\circ \rightarrow 3^\circ) = k\ (2^\circ \rightarrow 1^\circ) \times \exp(27.4 \times 10^3/(RT)).$

B.2. Hydride transfer

$k\ (1^\circ \rightarrow 2^\circ) = \text{reference: estimated by optimization;}$
$k\ (1^\circ \rightarrow 1^\circ) = k\ (1^\circ \rightarrow 2^\circ) \times \exp(-37.2 \times 10^3/(RT));$
$k\ (1^\circ \rightarrow 3^\circ) = k\ (1^\circ \rightarrow 2^\circ) \times \exp(16.7 \times 10^3/(RT));$
$k\ (2^\circ \rightarrow 1^\circ) = k\ (1^\circ \rightarrow 2^\circ) \times \exp(-37.2 \times 10^3/(RT));$
$k\ (2^\circ \rightarrow 2^\circ) = k\ (1^\circ \rightarrow 2^\circ);$
$k\ (2^\circ \rightarrow 3^\circ) = k\ (1^\circ \rightarrow 2^\circ) \times \exp(16.7 \times 10^3/(RT));$
$k\ (3^\circ \rightarrow 1^\circ) = k\ (1^\circ \rightarrow 2^\circ) \times \exp(-37.2 \times 10^3/(RT));$
$k\ (3^\circ \rightarrow 2^\circ) = k\ (1^\circ \rightarrow 2^\circ);$
$k\ (3^\circ \rightarrow 3^\circ) = k\ (1^\circ \rightarrow 2^\circ) \times \exp(-3.75 \times 10^3/(RT));$
$k\ (1^\circ \rightarrow \text{Allylic}) = k\ (1^\circ \rightarrow 2^\circ) \times \exp(16.7 \times 10^3/(RT));$
$k\ (2^\circ \rightarrow \text{Allylic}) = k\ (1^\circ \rightarrow 2^\circ) \times \exp(16.7 \times 10^3/(RT));$
$k\ (3^\circ \rightarrow \text{Allylic}) = k\ (1^\circ \rightarrow 2^\circ) \times \exp(-3.75 \times 10^3/(RT)).$

References

[1] S. Katare, A. Bhan, J.M. Caruthers, W.N. Delgass, V. Venkatasubramanian, Comput. Chem. Engin. 28 (2004) 2569.
[2] T.-Y. Park, G.F. Froment, Comput. Chem. Engin. 12 (1998) S103.
[3] W.O. Haag, R.M. Dessau, in: Proc. 8th Int. Congr. on Catalysis, Berlin, vol. 2, Verlag Chemie, Weinheim, 1984, p. 305.
[4] H. Krannila, W.O. Haag, B.C. Gates, J. Catal. 135 (1992) 115.
[5] T.F. Narbeshuber, H. Vinek, J.A. Lercher, J. Catal. 157 (1995) 388.
[6] J. Bandiera, Y.B. Taarit, Appl. Catal. 62 (1990) 309.
[7] B.S. Kwak, W.O. Haag, W.H.M. Sachtler, J. Catal. 149 (1994) 465.
[8] C. Stefanadis, B.C. Gates, W.O. Haag, J. Mol. Catal. 67 (1991) 363.
[9] W.K. Hall, E. Lombardo, J. Engelhardt, J. Catal. 115 (1989) 611.
[10] P.V. Shertukde, G. Marcelin, G.A. Sill, W.K. Hall, J. Catal. 136 (1992) 446.
[11] A. Corma, J.B. Monton, A.V. Orchilles, Appl. Catal. 16 (1985) 59.
[12] S. Kotrel, H. Knozinger, B.C. Gates, Micropor. Mesopor. Mater. 35–36 (2000) 11.
[13] F. Jentoft, B.C. Gates, Top. Catal. 4 (1997) 1.
[14] S.R. Blaszkowski, A.P.J. Jansen, M.A.C. Nascimento, R.A. van Santen, J. Phys. Chem. 98 (1994) 12938.
[15] V.B. Kazansky, M.V. Frash, R.A. van Santen, Catal. Lett. 28 (1994) 211.
[16] V.B. Kazansky, I.N. Senchenya, M.V. Frash, Catal. Lett. 27 (1994) 345.
[17] S.J. Collins, P.J. O'Malley, Chem. Phys. Lett. 246 (1995) 555.
[18] S.R. Blaszkowski, M.A.C. Nascimento, R.A. van Santen, J. Phys. Chem. 100 (1996) 3463.
[19] V.B. Kazansky, M.V. Frash, R.A. van Santen, Stud. Surf. Sci. Catal. 101 (1996) 1233.
[20] S.A. Zygmunt, L.A. Curtiss, P. Zapol, L.E. Iton, J. Phys. Chem. B 104 (2000) 1944.
[21] M.T. Aronson, R.J. Gorte, W.E. Farneth, D. White, J. Am. Chem. Soc. 111 (1989) 840.
[22] J.F. Haw, B.R. Richardson, B.R. Oshiro, N.D. Lazo, J.A. Speed, J. Am. Chem. Soc. 111 (1989) 2052.
[23] V.B. Kazansky, I.N. Senchenya, J. Catal. 119 (1989) 108.
[24] V.B. Kazansky, Acc. Chem. Res. 24 (1991) 379.
[25] P. Viruela-Martin, C.M. Zicovich-Wilson, A. Corma, J. Phys. Chem. 97 (1993) 13713.
[26] E.M. Evleth, E. Kassab, H. Jessri, M. Allavena, L. Montero, L.R. Sierra, J. Phys. Chem. 100 (1996) 11368.
[27] A. Bhan, Y.V. Joshi, W.N. Delgass, K.T. Thomson, J. Phys. Chem. B 107 (2003) 10476.
[28] J.B. Nicholas, T. Xu, J.F. Haw, Top. Catal. 6 (1998) 141.
[29] V.B. Kazansky, Stud. Surf. Sci. Catal. 85 (1994) 251.
[30] J.A. Lercher, K. Seshan, Curr. Opin. Solid State Mater. Sci. 2 (1997) 57.
[31] A. Corma, Curr. Opin. Solid State Mater. Sci. 2 (1997) 63.
[32] R.A. van Santen, Stud. Surf. Sci. Catal. 85 (1994) 273.
[33] R.J. Quann, S.B. Jaffe, Ind. Eng. Chem. Res. 31 (1992) 2483.
[34] G.F. Froment, Catal. Today 52 (1999) 153.
[35] W. Feng, E. Vynckier, G.F. Froment, Ind. Eng. Chem. Res. 32 (1993) 2997.
[36] G. Martens, G.F. Froment, Stud. Surf. Sci. Catal. 122 (1999) 333.
[37] J.A. Dumesic, D.F. Rudd, L.M. Aparicio, J.E. Rekoske, A.A. Trevino, The Microkinetics of Heterogeneous Catalysis, American Chemical Society, Washington, DC, 1993.
[38] G. Yaluris, J.E. Rekoske, L.M. Aparicio, R.J. Madon, J.A. Dumesic, J. Catal. 153 (1995) 54.
[39] G. Yaluris, J.E. Rekoske, L.M. Aparicio, R.J. Madon, J.A. Dumesic, J. Catal. 153 (1995) 65.
[40] M.A. Sanchez-Castillo, N. Agarwal, C. Miller, R.D. Cortright, R.J. Madon, J.A. Dumesic, J. Catal. 205 (2002) 67.
[41] M.A. Sanchez-Castillo, N. Agarwal, A. Bartsch, R.D. Cortright, R.J. Madon, J.A. Dumesic, J. Catal. 218 (2003) 88.

[42] D.B. Lukyanov, V.I. Shtral, Preprints of Symposium on Alkylation, Aromatization, Oligomerization, and Isomerization of Short-Chain Hydrocarbon over Heterogeneous Catalysts 36 (1991) 693.
[43] D.B. Lukyanov, N.S. Gnep, M.S. Guisnet, Ind. Eng. Chem. Res. 33 (1994) 223.
[44] D.B. Lukyanov, N.S. Gnep, M.S. Guisnet, Ind. Eng. Chem. Res. 34 (1995) 516.
[45] D.B. Lukyanov, Stud. Surf. Sci. Catal. 122 (1999) 299.
[46] D.B. Lukyanov, Stud. Surf. Sci. Catal. 105 (1997) 1301.
[47] J.M. Caruthers, J.A. Lauterbach, K.T. Thomson, V. Venkatasubramanian, C.M. Snively, A. Bhan, S. Katare, G. Oskarsdottir, J. Catal. 216 (2003) 98.
[48] B.H. Wojciechowski, Ind. Eng. Chem. Res. 36 (1997) 3323.
[49] G.F. Froment, K.B. Bischoff, Chemical Reactor Analysis and Design, Wiley, New York, 1990.
[50] F. Eder, J.A. Lercher, J. Phys. Chem. 100 (1996) 16460.
[51] F. Eder, M. Stockenhuber, J.A. Lercher, Stud. Surf. Sci. Catal. 97 (1995) 495.
[52] F. Eder, M. Stockenhuber, J.A. Lercher, J. Phys. Chem. B 101 (1997) 5414.
[53] F. Eder, J.A. Lercher, Zeolites 18 (1997) 75.
[54] E.G. Derouane, Chem. Phys. Lett. 142 (1987) 200.
[55] E.G. Derouane, J. Mol. Catal. A: Chem. 134 (1998) 29.
[56] L. Yang, K. Trafford, O. Kresnawahjuesa, J. Sepa, R.J. Gorte, D. White, J. Phys. Chem. B 105 (2001) 1935.
[57] S.M. Babitz, B.A. Williams, J.T. Miller, R.Q. Snurr, W.O. Haag, H. Kung, Appl. Catal. A: Gen. 179 (1999) 71.
[58] J.A. von Bekhoven, B.A. Williams, W. Ji, D.C. Koningsberger, H.H. Kung, J.T. Miller, J. Catal. 224 (2004) 50.
[59] B. Hunger, M. Heuchel, L.A. Clark, R.Q. Snurr, J. Phys. Chem. B 106 (2002) 3882.
[60] B. Smit, T.L.M. Maesen, Nature 374 (1995) 42.
[61] D.S. Santilli, T.V. Harris, S.I. Zones, Micropor. Mater. 1 (1993) 329.
[62] E.G. Derouane, C.D. Chang, Micropor. Mesopor. Mater. 35–36 (2000) 425.
[63] J.B. Nicholas, J.F. Haw, J. Am. Chem. Soc. 120 (1998) 11804.
[64] T. Xu, J.F. Haw, J. Am. Chem. Soc. 116 (1994) 7753.
[65] P.W. Goguen, T. Xu, D.H. Barich, T.W. Skloss, W. Song, Z. Wang, J.B. Nicholas, J.F. Haw, J. Am. Chem. Soc. 120 (1998) 2650.
[66] T. Xu, D.H. Barich, P.W. Goguen, W. Song, Z. Wang, J.B. Nicholas, J.F. Haw, J. Am. Chem. Soc. 120 (1998) 4025.
[67] I. Kiricsi, H. Forster, G. Tasi, J.B. Nagy, Chem. Rev. 99 (1999) 2085.
[68] M. Boronat, C.M. Zicovich-Wilson, P. Viruela, A. Corma, J. Phys. Chem. B 105 (2001) 11169.
[69] A.M. Rigby, M.V. Frash, J. Mol. Catal. A: Chem. 126 (1997) 61.
[70] V.B. Kazansky, Catal. Today 51 (1999) 419.
[71] J. Weitkamp, P.A. Jacobs, J.A. Martens, Appl. Catal. 8 (1983) 123.
[72] J.S. Buchanan, J.S. Santiesteban, W.O. Haag, J. Catal. 158 (1996) 279.
[73] V.B. Kazansky, M.V. Frash, R.A. van Santen, Catal. Lett. 48 (1997) 61.
[74] V.B. Kazansky, M.V. Frash, R.A. van Santen, Stud. Surf. Sci. Catal. 105 (1997) 2283.
[75] M. Boronat, P. Viruela, A. Corma, J. Phys. Chem. B 103 (1999) 7809.
[76] M. Boronat, P. Viruela, A. Corma, Phys. Chem. Chem. Phys. 2 (2000) 3327.
[77] T.C. Tsai, S.B. Liu, I.K. Wang, Appl. Catal. A: Gen. 181 (1999) 355.
[78] J. Cejka, B. Wichterlova, Catal. Rev.-Sci. Eng. 44 (2002) 375.
[79] M.A. Uguina, J.L. Sotelo, D.P. Serrano, J.L. Valverde, Ind. Eng. Chem. Res. 32 (1993) 49.
[80] Y. Xiong, P.G. Rodewald, C.D. Chang, J. Am. Chem. Soc. 117 (1995) 9427.
[81] X. Rozanska, X. Saintigny, R.A. van Santen, F. Hutschka, J. Catal. 202 (2001) 141.
[82] X. Rozanska, R.A. van Santen, F. Hutschka, J. Phys. Chem. B 106 (2002) 4652.
[83] M.S. Guisnet, N.S. Gnep, F. Alario, Appl. Catal. A: Gen. 89 (1992) 1.
[84] P. Meriaudeau, C. Naccache, Catal. Rev.-Sci. Eng. 39 (1997) 5.
[85] F.G. Oliver, E.J. Munson, J.F. Haw, J. Phys. Chem. 96 (1992) 8106.
[86] J.F. Haw, J.B. Nicholas, W. Song, F. Deng, Z. Wang, T. Xu, C.S. Heneghan, J. Am. Chem. Soc. 122 (2000) 4763.
[87] Y.V. Joshi, A. Bhan, K.T. Thomson, J. Phys. Chem. B 108 (2004) 971.
[88] Y.V. Joshi, K.T. Thomson, J. Catal. 230 (2005) 449.
[89] Y.V. Joshi, K.T. Thomson, unpublished results.
[90] S. Katare, J.M. Caruthers, W.N. Delgass, V. Venkatasubramanian, Ind. Eng. Chem. Res. 43 (2004) 3484.
[91] H. Rabitz, M. Kramer, D. Dacol, Ann. Rev. Phys. Chem. 34 (1983) 419.
[92] T. Turanyi, J. Math. Chem. 5 (1990) 203.
[93] C.T. Campbell, Top. Catal. 1 (1994) 353.
[94] P. Englezos, N. Kalogerakis, Applied Parameter Estimation for Chemical Engineers, Dekker, New York, 2000.
[95] D.A. Ratkowsky, Nonlinear Regression Modeling: A Unified Practical Approach, Dekker, New York, 1983.
[96] J.C. Nash, M. Walker-Smith, Nonlinear Parameter Estimation: An Integrated System in BASIC, Dekker, New York, 1987.
[97] D.C. Montgomery, G.C. Runger, Applied Statistics and Probability for Engineers, Wiley Text Books, New York, 2002.
[98] S.M. Campbell, D.M. Bibby, J.M. Coddington, R.F. Howe, R.H. Meinhold, J. Catal. 161 (1996) 338.
[99] G.L. Woolery, G.H. Kuehl, H.C. Timken, A.W. Chester, J.C. Vartuli, Zeolites 19 (1997) 288.
[100] M. Muller, G. Harvey, R. Prins, Micropor. Mesopor. Mater. 34 (2000) 135.
[101] I.I. Ivanova, E.B. Pomakhina, A.I. Rebrov, E.G. Derouane, Top. Catal. 6 (1998) 49.
[102] W.O. Haag, R. Lago, P. Weisz, Faraday Discuss. 72 (1981) 317.
[103] R.J. Correa, C.J.A. Mota, Phys. Chem. Chem. Phys. 4 (2002) 375.
[104] I.I. Ivanova, A.I. Rebrov, E.B. Pomakhina, E.G. Derouane, J. Mol. Catal. A: Chem. 141 (1999) 107.
[105] M. Seiler, U. Schenk, M. Hunger, Catal. Lett. 62 (1999) 139.
[106] J.A. Biscardi, E. Iglesia, J. Phys. Chem. B 102 (1998) 9284.
[107] J.A. Lercher, R.A. van Santen, H. Vinek, Catal. Lett. 27 (1994) 91.
[108] J.A. Biscardi, E. Iglesia, Catal. Today 31 (1996) 207.
[109] S.Y. Yu, J.A. Biscardi, E. Iglesia, J. Phys. Chem. B 106 (2002) 9642.
[110] T.F. Narbeshuber, M. Stockenhuber, A. Brait, K. Seshan, J.A. Lercher, J. Catal. 160 (1996) 183.
[111] T.F. Narbeshuber, A. Brait, K. Seshan, J.A. Lercher, J. Catal. 172 (1997) 127.
[112] S.R. Blaszkowski, R.A. van Santen, Top. Catal. 4 (1997) 145.
[113] P.M. Esteves, M.A.C. Nascimento, C.J.A. Mota, J. Phys. Chem. B 103 (1999) 10417.